Near-bottom Horizontal Transfer of Particulate Matter in the Palamós Submarine Canyon (NW Mediterranean)

J. Martín*, A. Palanques and P. Puig

Institut de Ciències del Mar, CMIMA-CSIC. Departament de Geologia Marina i Oceanografia Física. Passeig Marítim de la Barceloneta, 37-49,Barcelona, E- 08003, Spain.

Keywords: particulate flux; continental margins; ocean circulation; submarine canyon; northwestern Mediterranean Sea; Palamós Canyon (41-42ºN, 3-4ºE)

* Corresponding author. Tel.: +34-932309523 ; fax: +34-932309555.

E-mail address: jmartin@icm.csic.es

Cite as:

Martín, J., Palanques, A., Puig, P. 2007. Horizontal transfer of suspended particulate matter in the Palamós submarine canyon. Journal of Marine Research, 65(2): 193-218.

ABSTRACT

From March to November 2001, six current meters equipped with turbidimeters were moored 12 meters above the bottom inside the Palamós submarine canyon and on the adjacent slope. Horizontal particle fluxes were calculated from current and suspended sediment concentration data. This work aims to evaluate the advective sediment fluxes taking place in the Palamós canyon region, and to discern the nature and time-scales of the processes involved in the across-margin transfer of particles over the study period. Near-bottom currents inside the canyon were constrained by the local topography and displayed a high spatio-temporal variability. The net near-bottom transport of suspended matter in the canyon was largely driven by sharp increases of sediment load and current speed, most of them attributed to sediment gravity flows. These energetic events dominated over the current-driven sediment transport, which was relatively weak due to periodical up-canyon/down-canyon inversions along the canyon axis, and to complex current patterns and the presence of low sediment loads for most of the time at the other sites. During this 8-month experiment, the mid-canyon (> 1200 m depth) acted as a by-pass zone, while at the canyon head, net sediment transport was directed persistently up-canyon. These patterns were further heightened during a major storm in November 2001. However, in this particular submarine canyon, substantial sedimentary activity and offshore export of particulate matter also occur in the absence of significant external forcings (storms, river floods). Human activities (deep trawling) induced sediment gravity flows during the dry and calm season (spring-summer) and enhanced the offshore transfer of particles during this time period.

1. Introduction

The dynamics and fate of particulate matter on continental margins are of paramount importance in research topics such as the dispersion of contaminants or the fertilization of benthic ecosystems. It is widely accepted that to improve the understanding of the oceanic biogeochemical cycles, special attention must be paid to exchanges of matter and energy acting across margins. Studies of particle dynamics on continental margins around the world (Biscaye *et al.*, 1994; Etcheber *et al.*, 1996; Wong *et al.*, 2000; Wollast and Chou, 2001; Palanques *et al.*, 2002) have revealed that the main particle inputs to the mid- and lower slope are supplied by lateral transport from the shelf and upper slope rather than by pelagic settling.

Submarine canyons are preferential pathways for the effective transport of particulate matter across continental margins (Gardner, 1989; Puig and Palanques, 1998a; Hung *et al.*, 2003). In comparison with non-dissected open slopes, submarine canyons represent an abrupt interface of enhanced across-margin fluxes of water and particles. Firstly, the usual dendritic shape of canyons increases the effective length of the shelf-break and hence the scope for across-margin exchanges. Secondly, the rapid bathymetric changes may affect the regional circulation, eventually by-passing the coupled effect of density fronts and associated slope currents which tend to inhibit cross-shelf exchanges on many continental margins (Huthnance, 1995; Skliris *et al.*, 2002).

Inside canyons, particulate matter is usually concentrated in nepheloid layers and transported within the water flow (Gardner, 1989; Puig and Palanques, 1998b; van Weering *et al.*, 2002), but turbidity currents, episodes of axis-flushing and other gravitational processes can be crucial in determining the net offshore transport on longer time scales (May

et al., 1983; Mulder *et al.*, 2001; Xu *et al.*, 2002). Turbidity currents have usually been associated with geological periods of low sea level, when voluminous quantities of terrigenous sediments were conveyed to the deep basins through submarine canyons. However, the occurrence of intense turbidity currents in the present sea level high-stand is documented through indirect observations (see Nisbet and Piper, 1998, for a review), and more recently by direct observations in submarine canyons (Khripounoff *et al.*, 2003; Paull *et al.*, 2003; Xu *et al.*, 2004). Apart from the major events that have traditionally been regarded as turbidity currents, sediment gravity flows of less power but higher frequency do occur nowadays in environments such as submarine canyons, with steep bathymetries and major sediment accumulation (Shepard *et al.*, 1979; Puig *et al.*, 2004). Recent studies have confirmed that gravitational processes of moderate intensity act on some contemporary canyons with frequencies higher than was previously thought (Xu *et al.*, 2002; Puig *et al.*, 2003, 2004) and may thus constitute a major contributor to the offshore transport of matter in these regions.

In the last few decades, the flow over the continental margin and submarine canyons off the NE Spanish coast has been studied by means of SST telemetry (Masó *et al.*, 1990), synthetic aperture radar (Shirasago, 1996), drifting buoys (e.g. Sánchez-Velasco and Shirasago, 1999), vessel-mounted acoustic Doppler current profilers (Castellón *et al.*, 1990; Rojas *et al.*, 1995), CTD profiles (Alvarez *et al.*, 1996; García-Ladona *et al.*, 1996) and moored current meters (Font, 1990; Font *et al.*, 1995). However, most of these studies were restricted either to the surface flow or at best to the first few hundred meters of the water column. Published studies involving measurements of both vertical (sediment traps) and horizontal (current meters + turbidity sensors) fluxes of particulate matter near the bottom are

scarce in this region. To our knowledge, they are restricted to the Foix Canyon and the slope off Barcelona (Puig *et al.*, 2000).

In the context of the CANYONS project, six mooring arrays equipped with near-bottom sets of sediment traps, current meters and turbidimeters were deployed inside the Palamós submarine canyon and on the adjacent slope (Palanques *et al.*, 2005). Sediment traps were used to measure the downward fluxes and to determine the composition of settling particles in the canyon and its vicinity (Martín *et al.*, 2006). The present work aims to complement these results with a study of the horizontal component of near-bottom particle fluxes.

2. Study Area

The continental margin along the NE Spanish coast, from 42.3N to 41N, is characterized by a relatively narrow shelf dissected by two major incisions: the Palamós Canyon and the Blanes Canyon (Fig. 1). Both cut through almost the whole margin width, heading up to a few kilometers from the coast line, which contrasts with the relatively wide shelf in most of the Gulf of Lions, indented unevenly on its outer edge by numerous submarine canyons. The Palamós Canyon (Figs. 1 and 2), also known as La Fonera Canyon (Serra, 1981), stretches up to 40 km till it merges with the NW Mediterranean deep basin at 2000-2200 m depth. Its bifurcated head incises the continental shelf at the 90 m depth contour, 3 km away from the coastline, and the 1000 m isobath is located about 10 km from the coast. The canyon head, roughly oriented in a north-south direction, leads to a narrow axis oriented in a WNW-ESE direction, which gradually broadens towards the open sea. The steep canyon walls are indented by deep gullies (tributaries).

The general water circulation in the area is governed by a baroclinic current that follows the continental slope from NE to SW, in quasi-geostrophic equilibrium with a shelf/slope density front established between continental and open sea waters (Font *et al.*, 1988). This current is considered part of a greater continuum referred to as the Northern Current (NC) (Millot, 1999). Although the NC is confined to the upper 300-400 m of the water column, the general cyclonic circulation in the northwestern Mediterranean (Fig. 1), and hence the approximately SW flow direction in the study area, are considered to extend also to intermediate and deep water masses (Millot, 1999). The Ter River, which opens to the sea about 10 km north from the Palamós canyon head, is the most important stream on the nearby coast. The mean annual water discharge of this river at Girona (35 km upstream of the river mouth) is 17 m^3 s^{-1}, although water discharges can surpass 1000 m^3 s^{-1} when river floods occur.

3. Methodology

a. Field work

The geographical locations and depths of the mooring lines deployed inside and nearby the Palamós Canyon are illustrated in Figure 2 and detailed in Table 1. Three moorings were deployed in the canyon axis at nominal depths of 470, 1200 and 1700 m (M2, M3 and M5 respectively), two near the canyon walls at 1300 m depth (M4, north wall; M6, south wall), and one (M7) outside the canyon at 1300 m depth, on the open slope 15 km NE from the canyon axis. The study extended from March to November 2001, and was divided into two consecutive deployments: March 14th to July 11th and July 13th to November 28th. These dates varied in a range of 1-3 days for each mooring. M5 was accidentally released a few days after

the second deployment and redeployed successfully on July 31st. Each mooring line sustained an Aanderaa recording current meter (RCM-9) at 12 meters above the bottom (mab), set at a 10-minute sampling rate. RCM-9 units use a vector averaging method to record the speed and direction of the current, which are measured by means of the Doppler Shift principle. The current meters were also equipped with turbidity sensors. Current meter/turbidimeter pairs will be hereafter referred to with the same name as their respective moorings (Fig. 2). There were some gaps in the time series due to technical malfunctions and exhaustion of batteries: current meters M3 and M5 ceased to function on August 4th and August 31st respectively, while M7 worked only during the second deployment.

b. Current meter data processing

Current speeds and directions were decomposed in east-west and north-south directions. The resulting velocity components were also rotated to match a local reference system of across- and along-canyon directions. Due to the complex topography in the study area, and hence the variable orientation of the sampling sites with respect to bathymetric gradients, a specific rotation was chosen for each particular case. Moorings M2, M3 and M5 were rotated to match the mean orientation of the axis at each location (anticlockwise from the north: 10º, 75º and 67.5º respectively). At the moorings deployed near the canyon walls (M4 and M6), the along-canyon direction was defined parallel to the local isobaths, resulting in a rotation of 67.5 º for M4 and 45º for M6. The positive direction of the rotated vectors is up-canyon in the along-canyon direction and upstream (in relation to the mean regional flow, which is roughly SSW) in the across-canyon direction. Data from the open slope site M7 was rotated 67.5º (always anticlockwise from the north) in order to match an approximate along/across-margin reference system, with positive directions shoreward (ESE) and upstream (NNE).

c. Turbidimeter calibration

Aanderaa turbidimeters express the light-scattering intensity as equivalent Nephelometric Turbidity Units (NTU). In order to convert the NTU output into concentration of suspended matter, a field calibration was carried out during an oceanographic cruise conducted in the study area, by attaching an RCM-9/turbidimeter to a rosette of Niskin bottles. Several vertical profiles were conducted while water samples were collected at different depths. The water samples were vacuum-filtered up to filter saturation onto pre-weighed Nucleopore filters of 0.4 μm pore size. The weight of the dry residue, divided by the volume of water filtered, rendered suspended sediment concentration (SSC) in units of mg l^{-1}. Pairs of NTU/SSC data points from depths ranging between 50 m and 1800 m depth yielded the following linear regression:

$$SSC\ (mg\ l^{-1}) = 0.99 \cdot NTU + 0.02 \qquad (n = 46\ ;\ R^2 = 0.77)$$

However, all the measurements during the calibration were < 1.5 NTU, whereas turbidity increases in the Palamós canyon reached several tens of NTU. For a wider turbidity range, Guillén *et al.* (2000) obtained the following general calibration for the northwestern Mediterranean:

$$SSC\ (mg\ l^{-1}) = 1.74 \cdot NTU - 1.32 \qquad (n = 133\ ;\ R^2 = 0.99)$$

These two linear regressions intersect at NTU = 2. As most of the turbidity values used by Guillen *et al.* (2000) are substantially higher than those recorded in this study, our calibration

was deemed more accurate for lower turbidity values. Therefore, our calibration was used to transform turbidity data < 2 NTU and the calibration of Guillén *et al.* (2000) for values above 2 NTU.

d. Calculation of horizontal particle fluxes

Suspended particulate matter is constituted by particles that are unable to settle without some ballasting effect (Honjo, 1996). Settling particles are in comparison much rarer in the water column due to their lower residence time. Furthermore, backscatter sensors are more sensitive to fine than to coarse grain sizes (Bunt *et al.*, 1999). Therefore, it can be assumed that the output of the backscatter sensors was largely attributable to suspended particles. Assuming that these particles move with the velocity of the water within which they are suspended (Wright, 1995), the horizontal particle flux or suspended sediment flux (SSF) in mg m^{-2} s^{-1} can be obtained as the product of the velocity module and the SSC, with the same direction as the flow. Fluxes were rotated into the along-/across-canyon (across-/along-margin in the open slope case) coordinate system in the same manner as current data.

e. Auxillary data

Wave data were provided by a buoy belonging to the REMRO network of oceanographic buoys of "Puertos del Estado" (Spanish Ports Authority). This buoy is located at 41º49.8'N, 3º11.2'E, 7 km SW of the Palamós Canyon's southern rim, over the 90 m isobath. A WANA point (daily wave forecast output from the fourth generation wave model used by "Puertos del Estado" along the NE Spanish coast) was used to fill gaps in the buoy time series. We chose the WANA point at 41º52.5'N, 3º15.0'E due to its proximity to both the oceanographic

buoy and the canyon. The daily discharge of the Ter River was supplied by "Agència Catalana de l'Aigua" (Catalan Government Water Agency), comprising the sum of the daily flow of the river at the Girona gauging station and that of its main downstream tributary, the Onyar River.

4. Results

a. General forcing conditions during the study

During most of the study period, there were neither major storms nor river floods. From March to early November, significant wave height (H_s) and peak period (T_p) never exceeded 3 m and 9 s respectively, while the Ter River discharge was always below 8 m^3 s^{-1} (Fig. 3), which is under its mean annual discharge. However, near the end of the deployment period, a severe storm struck the northwestern Mediterranean from November 11th to approximately November 20th 2001. During the peak of the storm, the buoy near Palamós Canyon ceased to function but the WANA model predicted H_S > 11 m and T_P > 12 s at a nearby point (Fig. 3). The return period of a storm like this has been estimated as 20 years (Ibarra Damiá and Medina, 2003). Even during the major storm, the Ter River discharge was only ~ 11 m^3 s^{-1}.

b. Currents

Table 2 shows maximum and mean current speeds recorded by current meters for two different conditions, according to the previous section: relatively calm conditions from March to early-November and a major storm and its aftermath in mid- and late-November. The mean current vectors or net flows derived from the average north and east component of the

current velocity are depicted in Figure 4, separated into the two general ambient conditions indicated above. Figure 5 illustrates the progressive plots of the current meters.

Near-bottom currents (Figs. 4 and 5) were highly variable and apparently decoupled from the regional circulation (approximately directed towards the SW) at all the sites. Along the canyon axis, currents were clearly constrained by the topography and forced to flow preferentially in an along-axis direction, with frequent up/down-canyon inversions (Fig. 5), as is usually observed in submarine canyons around the world (e.g. Shepard *et al.*, 1979; Csanady *et al.*, 1988; Puig *et al.*, 2000). At the other canyon sites and at the open slope site, the flow was also greatly influenced by the local bottom morphology. Spectral analysis of the near-bottom current series (Palanques *et al.*, 2005) revealed two main spectral peaks identified as the inertial frequency at 18.07 h, and a second oscillation with T~3 days, which was attributed to a topographic wave (Palanques *et al.*, 2005).

The net near-bottom water motion along the canyon axis was directed up-canyon at 1700 (M5), 1200 (M3) and 470 (M2) m depth (Fig. 4a). However, the mean current vectors were veered to the left of the actual orientation of the axis, heading up-canyon (Fig. 4a), which could be attributable to Ekman veering. The effect of Ekman veering has been noticed before in the turbulent bottom boundary layer inside submarine canyons (Hunkins, 1988; Xu *et al.*, 2002), by comparing the current directions of current meters deployed at several heights (from a few meters to tens of meters) above bottom. Although we do not have vertical resolution, Ekman veering at the depth of our near-bottom instruments (12 mab) is likely to occur.

Near-bottom currents were significantly stronger at the north than at the south canyon wall (Table 2). This would lead to preferential accumulation of particulate matter at the southern wall, since particles kept in suspension by turbulence may settle out of the water column as the current weakens. This assumption is in concordance with downward fluxes measured by the sediment traps which accompanied these current meters (Martín *et al.*, 2006).

Currents at the open slope site M7 had lower variability than those observed in the canyon at similar depths. The current at M7 alternated between two main flow directions: one roughly oriented offshore (ESE), which was dominant during most of the study period, and one oriented roughly SW, which predominated during the stormy period (Fig. 5).

The net flows shown in Figure 4 are relatively weak due to the strong current variability and, in the particular case of the along-axis sites, to periodical up-canyon/down-canyon current inversions, whose frequency increased shoreward from M5 to M2 (Fig. 5).

c. Suspended particulate matter fluxes

Figures 6 to 11 illustrate suspended sediment fluxes (SSF) calculated from the rotated current components in the along- and across-canyon directions (across- and along-margin directions at the open slope site), and cumulative mass transport, calculated as the cumulative sum of rotated fluxes.

Most of the time, the transport of suspended particles illustrated in Figures 6-11 was in agreement with the mean water flows depicted in Figure 4. However, at several sites inside the canyon, despite their relatively short duration (range of hours), sporadic pulses of high

particle flux controlled the total cumulative transport during the deployment period. At M5 (Fig. 8), a steady trend of up-canyon cumulative sediment transport was disrupted in mid-August by two events of sharp flux increase, which turned the cumulative mass transport down-canyon and increased it by two orders of magnitude in a matter of hours (Fig. 8). At M3, the flux peaks were less intense but more frequent than at M5 (Figs. 7, 8). During periods without extreme events, the cumulative mass transport at M3 was either directed up-canyon or almost balanced, but the flux peaks during events changed this pattern radically, leading to a strong down-canyon and especially downstream (SSW) sediment transport (Fig. 7). Also at the south canyon wall (Fig. 10), a single and brief sediment flux event in late spring largely dominated the cumulative mass transport over the 8-month study period. On the other hand, at the canyon head (Fig. 6), at the north canyon wall (Fig. 9), and at the open slope site (Fig. 11), no extreme sediment flux events were observed and the sediment transport was essentially governed by the net water flows (Fig. 4). The persistent up-canyon and westward sediment transport at M2 (Fig. 6) throughout the study suggests accumulation of particles in the canyon head, while net down-canyon/offshore sediment transport takes place at the rest of the canyon and slope sites.

5. Discussion

a. Sediment gravity flows

Most of the flux peaks controlling the horizontal sediment transport in Figs. 7, 8 and 10 shared common characteristics. Figures 12 and 13 illustrate some of these events in detail. The simultaneous bursts of SSC and current speed, together with the flow directions (always downslope, and sustained during the event), form the typical signature of a sediment gravity

flow. The generic term "sediment gravity flow" embraces any flow by which water moves due to the contribution of suspended sediment load to the density of the fluid, creating negative buoyancy (Middleton and Hampton, 1973, 1976).

During the last decades, several studies have recorded events of large bodies of sediment-water mixture flowing down the axis of submarine canyons in response to different mechanisms, such as hyperpycnal flows following river discharges with high sediment loads (Mulder and Syvitski, 1995; Mulder *et al.*, 1997; Johnson *et al.*, 2001), or mass failure on canyon walls caused by earthquakes (Garfield *et al.*, 1994; Okey, 1997). In those canyons whose head falls in the depth range of wave-induced stress, major storms are a prime process in initiating gravity-laden flows (Mulder *et al.*, 2001; Puig *et al.*, 2003, 2004; Xu *et al.*, 2004). Aside from natural forcing mechanisms, human activities like dumping of dredge material (Xu *et al.*, 2004) and trawling fisheries operating along canyon walls (Palanques *et al.*, 2006) can also trigger downcayon gravity flows. Moreover, in certain submarine canyons, exceptional triggering events may not be required (Paull *et al.*, 2003).

i. Sediment gravity flows at 1200 m depth in the canyon axis

Sediment gravity flows at 1200 m depth were very frequent and occurred mainly from May to August. Most of them were triggered by otter trawlers towing at depths of 400-800 m along the north canyon rim. A complete description of these anthropogenic sediment gravity flows is given in Palanques *et al.* (2006). Many of them reached the M3 site through a gully incised across the north wall, just above the M3 site (Palanques *et al.*, 2006). However, 3 of the major flux peaks in M3 advanced roughly towards the east (90º), that is, the down-canyon direction of the axis at this site (Fig. 2).

In Figure 12, three gravity flows representative of those coming from the north wall and triggered by trawlers, as described in Palanques *et al.* (2006), are compared with the 3 major events flowing along the canyon axis. The flux peaks on May 30th and July 28th occurred out of working hours and hence are not directly attributable to trawling activities. They arrived at M3 following an up-canyon/down-canyon inversion of the flow (Fig. 12b). In particular, the event of July 28th was not accompanied by a simultaneous increase in current speed, so a sediment gravity flow cannot be invoked in this case. Instead, it seems that the current inversion brought to the site a turbid water mass located up-canyon, whether or not this nepheloid layer had its origin in human-induced resuspension up-canyon from M3. On the contrary, the fishermen were trawling the northern canyon wall when the May 11th event (Fig. 12b) was recorded. Palanques *et al.* (2006) proposed that apart from the sediment gravity flows coming directly from the gully just above M3, others can be channeled towards the axis from gullies located up-canyon, and then reoriented along the canyon axis towards M3. It is noteworthy that the along-axis gravity flows (Fig. 12b) had similar values of SSC and current speed than the across-canyon gravity flows (Fig. 12a), but the peaks were sustained for longer times in the along-axis cases (Fig. 12), implying higher sediment transport per event. This has important implications for the redistribution of sediments in the canyon, meaning that, instead of rapidly fading away or colliding with the south canyon wall, the frequent across-canyon gravity flows detected at M3 may also be reoriented along the canyon axis, resuspending and entraining more sediment in their wake as the gravity flow advances downslope. However, the horizontal extent of these downslope flows must be limited, since none of the sediment gravity flows recorded at 1200 m depth (M3) were detected at 1700 m (M5) in the following hours.

ii. Sediment gravity flows at 1700 m depth in the canyon axis

Only two sediment gravity flows were recorded at 1700 m depth in the canyon axis. They occurred during August, approximately one week apart. The first one moved downslope along the canyon axis, while the second one was directed across-isobaths, apparently coming from the south canyon wall (Fig. 13a). The first one may also have flowed originally from the canyon walls up-canyon from the M5 site, and then reoriented after encountering the canyon axis. As observed in M3, the along-axis event was stronger than the across-canyon one in terms of horizontal transport of particles.

These two events were correlated with a sharp increase in the downward particle flux measured by the sediment trap during the same period (Fig. 13a). The compositional data of sediment trap samples suggested resuspension of reworked sediments (Martín *et al.*, 2006). During both events, current speeds reached up to 40 cm s^{-1} and the turbidity sensors were saturated by the high concentration of particles. Therefore, the maximum estimated SSC (~39 mg l^{-1}), and hence the fluxes calculated at M5 during these extreme events, should be regarded as minima. It must also be taken into account that RCM-9 velocity data represent a vector average every 10 min, so the actual instantaneous speeds may have been greater than those shown in Figure 13a. Furthermore, since our current and turbidity data were recorded at 12 mab, our observations may not represent exactly the head of the current, but instead lower fluxes, depending on the overall velocity structure. In situ observations of sediment gravity flows in the Monterey Canyon, showed that the head of the current (defined as the elevation of the speed maximum in the velocity profile) was located at 5-12 mab, becoming closer to the sea bed as the currents moved down-canyon (Xu *et al.* 2004).

A sediment core extracted in the Palamós canyon at 1700 m depth (M5) (Martín, 2005) revealed that the sediment accumulation rate has increased from the seventies, concurrently with the apparition of horizontal layering in the sediment column that may indicate successive events of fast deposition. This increased accumulation rate has been related to the technical improvements that trawling gears have experienced in the same period (from the 1960s-1970s to the present day). However, the two sediment gravity flows recorded in August 2001 cannot be directly linked to trawling activities since they occurred on non-working days and far from heavily-fished areas. During most of the study period, and particularly when sediment gravity flows occurred at 1200 m depth, the net particulate matter flux at the M5 site was up-canyon (excluding the two gravity flows in August). As some of the major suspended sediment fluxes at M3 flowed down-canyon and the rest to the south, there must be a pile-up of sediment at an intermediate location between these two mooring sites. Flushing of unstable sediment packages from this hypothetical accumulation area is a possible explanation for the deep sediment gravity flows observed at 1700 m depth, especially the event directed along the canyon axis.

iii. A sediment gravity flow at the south canyon wall

At the M6 site, only one gravity flow was observed during the study period (Fig. 13b), which nonetheless determined the cumulative mass transport at this site (Fig. 10). This sediment gravity flow occurred on May 31st, lasted for 3 hours and apparently came from the south canyon wall. The downward fluxes, measured by a sediment trap installed 10 m above the RCM-9, were not as markedly influenced by this event as in the case of M5 (Fig. 13a). This sediment gravity flow occurred while the local trawling fleet was operating at the south

canyon wall (Fig. 1 in Palanques *et al.*, 2006) and therefore could be human-induced like those at M3.

b. Suspended sediment fluxes during a major storm

Near-bottom current speed increased during the November storm at all sites where data was still being recorded (Table 2). During the storm, net water motion was higher on the open slope than at the canyon sites (Fig. 4), as a result not of higher instantaneous speeds but of a steadier current direction on the slope, in contrast with the strong current variability observed inside the canyon (Fig. 5), especially at M6, where high-frequency vorticity resulted in an almost negligible net water motion.

The horizontal sediment transport was enhanced during the storm at the canyon head (M2), the northern canyon wall (M4), and on the open slope (M7), whereas it was lower at the southern canyon wall (M6). The instruments at M3 and M5 failed prior to the storm. The influence of the November storm (estimated return period of 20 years) on the cumulative mass transport was relatively weak or insignificant (Figs. 6, 9, 10 and 11). During this major storm, no sediment gravity flows were observed at the canyon head (M2). Instead, the sediment flux was controlled by alternating up/down-canyon currents with a weak net advection, directed up-canyon and shoreward.

The storm contributed more significantly to increasing the downward particle fluxes collected in the sediment traps (Martín *et al.*, 2006) than the horizontal particle fluxes. In contrast with the relatively weak influence of this major storm on net horizontal sediment advection at the canyon head, the maximum values of downward particle fluxes occurred

during the storm at all the canyon sites (with the exception of M6), even overfilling the traps installed at M2 and M3 (Martín *et al.*, 2006). The energetic conditions during this storm introduced into the canyon coarser particles resuspended on the shelf, as proven by granulometric analysis of sediment trap samples (unpublished data). Coarser particles, with higher settling rates, are collected by the sediment trap but they are poorly recorded by the optical backscatter sensors (Bunt *et al.*, 1999), and this could lead to a lower detection of these particles by the turbidimeter during the storm period.

c. Mean horizontal fluxes of suspended particulate matter

Net suspended sediment fluxes (SSF) obtained from current meter/turbidimeter pairs are shown in Figure 14. A strong discordance between the directions of net water flows (Fig. 4) and net SSF (Fig. 14) is evident at several sites but especially at the canyon axis (M3, M5). Along the canyon axis, the mean current (water transport) was directed up-canyon (Figs. 4 and 6-8), but the sediment transport was quantitatively dominated by sediment gravity flows, directed down-canyon. The strong down-canyon net flux (55.5 mg m^{-2} s^{-1}) at 1700 m (Fig. 14a) was due solely to the two consecutive sediment gravity flows described in Section 4.4.2 and Figure 13a. Gravity flows also governed the net horizontal sediment flux at M6 (Figs. 10 and 14). The southward direction of M3 mean flux vectors (Fig. 14a) is explained by the fact that most gravity flows were channeled from a gully incised in the northern wall, just above the location of mooring M3 (Palanques *et al.*, 2006). The results suggest net offshore export in the distal part of the canyon ($\geq$ 1200 m depth) during the study period.

At the canyon head, the absence of significant sediment flux peaks like those observed at M3 or M5 caused the near-bottom net fluxes to follow approximately the direction of the

mean flow (see Figs. 4 and 14), that is, up-canyon and shoreward, suggesting retention of particles in the canyon head region (Fig. 6), especially during the storm when fluxes were considerably increased (Fig. 14b). This net flux at M2 was not the consequence of an unidirectional flux during the storm, but rather to the residual flux of an alternating up/down-canyon flow pattern at this site. One possible reason for the absence of gravity flows at M2 lies in the fact that this site was located upcanyon from the main fishing grounds exploited by the local trawling fishery (Palanques *et al.*, 2006).

6. Summary

The near-bottom currents observed in the Palamós submarine canyon were decoupled from the mean regional circulation and constrained by the bottom topography. Net water motion and net suspended sediment transport driven by currents was weak inside the canyon as a result of alternating up-canyon/down-canyon current inversions in the canyon axis, and of complex current patterns at the canyon walls. However, at 1200 and 1700 m depth in the canyon axis, and at 1300 m depth at the south canyon wall, sediment gravity flows occurred, enhancing the near-bottom horizontal transfer of particles by several orders of magnitude.

In contrast with the generally accepted scheme which attributes to canyon heads a function of catchment areas of particles in transit to the abyss, this canyon shows a peculiar trend in terms of advective sediment fluxes: the canyon head is a hydrodynamically confined area, apparently functioning as a trap or a recirculating area for particles. No sediment gravity flows were observed at the canyon head, even under a 20-year storm. The main sediment transport seems to take place through the steep canyon walls and their associated gullies, which convey shelf and upper slope resuspended material to deeper portions of the canyon

axis (1000-2000 m depth) by sediment gravity flows either of natural origin or triggered artificially by trawling activities. These across-canyon gravity flows may be reoriented along the canyon axis and advance further downslope, eventually resuspending more sediment along their path and enhancing offshore sediment transport.

This study shows that the role of steep and deeply incised canyons such as the Palamós Canyon as a trap or a channel for sediments depends largely on the time-scale considered, since the net transport is largely event-driven. Thus, a small temporal coverage may lead to unrepresentative results by only grasping particular conditions or—on the contrary—by reflecting a "normal" trend and missing single events that may amply govern the net sediment transport.

Our results also show that sediment gravity flows control the net horizontal transport of particulate matter in this particular submarine canyon, specially in spring and summer during "calm" conditions, i.e., in the absence of significant river discharges or storms. Furthermore, superimposed on natural processes, anthropogenic activities contributed significantly to the downslope transport of particulate matter in the Palamós Canyon during the study period, at least at 1200 m depth in the canyon axis. This finding raises the question whether human activities could have dramatically changed the patterns of particulate matter dispersion and accumulation in this and other submarine environments during the last few decades. The ecological consequences of this prospect are beyond the scope of this study but deserve further investigation by the scientific community.

Acknowledgments. This work was carried out in the framework of the CANYONS project funded by the Spanish National R+D Plan. The first author was funded during this

study by an FPI fellowship from the Spanish Ministry of Science and Technology (MCYT). We thank the officers and crew of the R/V García del Cid for their help during the deployment operations. The manuscript benefited greatly from the comments of Dr. Emilio García-Ladona and Dr. Jorge Guillén (ICM-CSIC), and the constructive criticism of three anonymous referees.

References

Alvarez, A., J. Tintoré and A. Sabatés. 1996. Flow modification and shelf-slope exchange induced by a submarine canyon off the northeast Spanish coast. J. Geophys. Res., 101, 12043-12055.

Biscaye, P.E., C.N. Flagg and P.G. Falkowsky. 1994. The Shelf Edge Exchange Processes experiment: SEEP-II: an introduction to hypotheses, results and conclusions. Deep-Sea Res. II, *41*, 231-252.

Bunt, J.A.C., P. Larcombe and C.F. Jago. 1999. Quantifying the response of optical backscatter devices and transmissometers to variations in suspended particulate matter. Cont. Shelf Res., *19*, 1199-1220.

Castellón, A., J. Font and E. García-Ladona. 1990. The Liguro-Provençal-Catalan Current (NW Mediterranean) observed by Doppler profiling in the Balearic Sea. Sci. Mar., *54*, 266-276.

Csanady, G.T., J.H. Churchill and B.Butman. 1988. Near-bottom currents over the continental slope in the Mid-Atlantic Bight. Cont. Shelf Res., *8*, 653-671.

Etcheber, H., S. Heussner, O. Weber, A. Dinet, X. Durrieu de Madron, A. Monaco, R. Buscail and J.C. Miquel. 1996. Organic carbon fluxes and sediment biogeochemistry on the French Mediterranean and Atlantic margins, *in* Particle Flux in the Ocean, SCOPE Report 57, V. Ittekkot, P. Schäfer, S. Honjo and P.J. Depetris, eds., John Wiley & Sons, 223-241.

Font, J., E. García-Ladona and E. García-Górriz. 1995. The seasonality of mesoscale motion in the Northern

Current of the western Mediterranean: several years of evidence. Oceanol. Acta, *18(2)*, 207-219.

Font, J. 1990. A comparison of seasonal winds with currents on the continental slope of the Catalan Sea (Northwestern Mediterranean). J. Geophys. Res., *95(C2)*, 1537-1545.

Font, J., J. Salat and J. Tintoré. 1988. Permanent features of the circulation in the Catalan Sea, in Pelagic Mediterranean Oceanography, Ed. H.J. Minas, P. Nival, Oceanol. Acta, vol. sp. *9*, 51-57.

García-Ladona, E., A. Castellón, J. Font and J. Tintoré. 1996. The Balearic current and volume transports in the Balearic basin. Oceanol. Acta, 19, 489-497.

Gardner, W.D. 1989. Baltimore Canyon as a modern conduit of sediment to the deep sea. Deep-Sea Res., *36*, 323-358.

Garfield, N., T.A. Rago, K.J. Schnebele and C.A. Collins, 1994. Evidence of a turbidity current in Monterrey Submarine Canyon associated with the 1989 Loma Prieta earthquake. Cont. Shelf Res., *14 (6)*, 673-686.

Guillén, J., A. Palanques, P. Puig, X. Durrieu de Madron and F. Nyffeler. 2000. Field calibration of optical sensors for measuring suspended sediment concentration in the western Mediterranean. Sci. Mar., *64(4*), 427-435.

Honjo, S. 1996. Fluxes of particles to the interior of the open oceans, *in* Particle Flux in the Ocean, SCOPE Report 57, V. Ittekkot, P. Schäfer, S. Honjo and P.J. Depetris, eds., John Wiley & Sons, 91-113.

Hung, J.-J., C.-S. Lin, Y.-C. Chung, G.-W. Hung and W.-S. Liu. 2003. Lateral fluxes of biogenic particles through the Min-Hua canyon in the southern East China Sea slope. Cont. Shelf Res., *23*, 935-955.

Hunkins, K. 1988. Mean and tidal currents in Baltimore canyon. J. Geophys. Res., *93*, 6917-6929.

Huthnance, J.M. 1995. Circulation, exchange and water masses at the ocean margin: the role of physical

processes at the shelf edge. Prog. Oceanogr., *35*, 353-431.

Ibarra Damiá, V. and J.R. Medina. 2003. Los temporales de Noviembre de 2001 en la costa Mediterránea: Obras de reparación en los puertos de Benicarló y Denia, *in* VII Jornadas Españolas de Ingeniería de Costas y Puertos. Libro de Resúmenes, M.A. Losada and M.C. Castillo, eds., Fundación para el Fomento de la Ingeniería del Agua, 364-366.

Johnson, K.S., C.K. Paull, J.P. Barry and F.P. Chavez. 2001. A decadal record of underflows from a coastal river into the deep sea. Geology, *29(11)*, 1019-1022.

Khripounoff, A., A. Vangriesheim, N. Babonneau, P. Crassous, B. Dennielou and B. Savoye. 2003. Direct observation of intense turbidity current activity in the Zaire submarine valley at 4000 m water depth. Mar. Geo., *194*, 151-158.

Martín, J., A. Palanques and P. Puig. 2006. Composition and Variability of Downward Particulate Matter Fluxes in the Palamós Submarine Canyon (NW Mediterranean). J. Mar. Syst., *60*, 75-97.

Martín, J. 2005. Sedimentary Dynamics in the Palamós Submarine Canyon. PhD Thesis. Universitat Politècnica de Catalunya, 198 pp.

Masó, M., P.E. La Violette and J. Tintoré. 1990. Coastal flow modification by submarine canyons along the NE Spanish Coast. Sci. Mar., *54(4)*, 343-348.

May, J.A., J.E. Warme and R.A. Slater. 1983. Role of submarine canyons on shelfbreak erosion and sedimentation: modern and ancient examples. SEPM Spec. Publ., *33*, 315-332.

Middleton, G.V. and M.A. Hampton. 1976. Subaqueous sediment transport and depositional by sediment gravity flows, *in* Sediment Transport and Environmental Management, D.J. Stanley and D.J.P. Swift, eds., John Wiley, 197-218.

Middleton, G.V. and M.A. Hampton. 1973. Sediment gravity flows; mechanics of flow and deposition, in Turbidites *in* Deep Water Sedimentation, G.V. Middleton and A.H. Bouma, eds., Society of Economical Paleontology Mineral Pacific Section Short Course Lecture Notes, 1-38.

Millot, C. 1999. Circulation in the Western Mediterranean Sea. J. Mar. Syst., *20*, 423-442.

Mulder, T., O. Weber, P. Anschutz, F.J. Jorissen and J.M. Jouanneau. 2001. A few months-old storm generated turbidite deposited in the Capbreton Canyon (Bay of Biscay, SW France). Geo-Mar. Lett., *21*, 149-156.

Mulder, T., B. Savoye, J.P.M. Syviski and O. Parize. 1997. Des courants de turbidité hyperpycnaux dans la tête du canyon du Var? Données hydrologiques et observations de terrain. Oceanol. Acta, *20 (4)*, 607-624.

Mulder, T. and J.P.M. Syvitski. 1995. Turbidity currents generated at river mouths during exceptional discharges to the world oceans. J. Geol., *103*, 285-299.

Nisbet, E.G. and D.J.W. Piper. 1998. Giant submarine landslides. Nature, *392*, 329-330.

Okey, T.A. 1997. Sediment flushing observations, earthquake slumping, and benthic community changes in Monterey Canyon head. Cont. Shelf Res., *17*, 877-897.

Palanques, A., J. Martín, P. Puig, J. Guillén, J.B. Company and F. Sardà. 2006. Evidence of sediment gravity flows induced by trawling in the Palamós (Fonera) submarine canyon (northwestern Mediterranean). Deep-Sea Res. I, *53*, 201-214.

Palanques, A., E. García-Ladona, D. Gomis, J. Martín, M. Marcos, A. Pascual, M. Emelianov, P. Puig, J. Guillén, J.M. Gili, J. Tintoré, A. Jordi, G. Basterretxea, J. Font, M. Segura, D. Blasco, S. Montserrat, S. Ruiz and F. Pages. 2005. A multidisciplinary program to study the dynamics and the ecology of a Northwestern Mediterranean submarine canyon: The Palamós Canyon. Prog. Oceanogr., *66(2-4)*, 89-119.

Palanques, A., E. Isla, P. Masqué, P. Puig, J.-A. Sánchez-Cabeza, J.M. Gili and J. Guillén. 2002. Downward

particle fluxes and sediment accumulation rates in the western Bransfield Strait: Implications of lateral transport for carbon cycle studies in Antarctic marginal seas. J. Mar. Res., *60*, 347-365.

Paull, C.K., W. Ussler, H.G. Greene, R. Keaten, P. Mitts and J. Barry. 2003. Caught in the act: the 20 December 2001 gravity flow event in Monterey Canyon. Geo-Mar. Lett., *22*, 227-232.

Puig, P., A.S. Ogston, C.A. Mullenbach, C.A. Nittrouer, J.D. Parsons and R.W. Sternberg. 2004. Storm-induced sediment gravity flows at the head of the Eel submarine canyon, northern California margin. J. Geophys. Res., *109(C3)*, C03019.

Puig, P., A.S. Ogston, B.L. Mullenbach, C.A. Nittrouer and R.W. Sternberg. 2003. Shelf-to-canyon sediment-transport processes on the Eel continental margin (northern California). Mar. Geo., *193*, 129-149.

Puig, P., A. Palanques, J. Guillén and E. García-Ladona. 2000. Deep slope currents and suspended particle fluxes in and around the Foix submarine canyon (NW Mediterranean). Deep-Sea Res. I, *47*, 343-366.

Puig, P. and A. Palanques. 1998a. Temporal Variability and composition of settling particle fluxes on the Barcelona continental margin (Northwestern Mediterranean). J. Mar. Res., *56*, 639-654.

Puig, P. and A. Palanques. 1998b. Nepheloid structure and hydrographic control on the Barcelona continental margin, Northwestern Mediterranean. Mar. Geo., *149*, 39-53.

Rojas, P., M.A. García, J. Sospedra, J. Figa, J. Puigdefàbregas, O. López, M. Espino, V. Ortiz, A. Sánchez-Arcilla, M. Manríquez and B. Shirasago. 1995. On the structure of the mean flow in the Blanes Canyon area (NW Mediterranean) during summer. Oceanol. Acta, *18*, 443-454.

Sánchez-Velasco, L. and B. Shirasago. 1999. Spatial distribution of some groups of microzooplankton in relation to oceanographic processes in the vicinity of a submarine canyon in the north-western Mediterranean Sea. Ices J. Mar. Sci., 56(1), 1-14.

Serra, J. 1981. Els canyons submarins del marge continental Català. Treb. Inst. Cat. Hist. Nat., *9*, 53-57.

Shepard, F.P., N.F. Marshall, P.A. McLoughlin and G.G. Sullivan. 1979. Currents in Submarine Canyons and Other Sea valleys. The American Association of Petroleum Geologists, 173 pp.

Shirasago, B. 1996. Aplicaciones del Radar de Apertura Sintética (SAR) del satélite ERS-1 al estudio de la dinámica superficial de mesoescala en el Mediterráneo Occidental. PhD Thesis. Universidad de Barcelona, 252 pp.

Skliris, N., J.H. Hecq and S. Djenidi. 2002. Water fluxes at an ocean margin in the presence of a submarine canyon. J. Mar. Syst., *32*, 239-251.

van Weering, T.C.E., H.C. de Stigter, W. Boer and H. de Haas. 2002. Recent sediment transport and accumulation on the NW Iberian margin. Prog. Oceanogr., *52*, 349-371.

Wollast, R. and L. Chou. 2001. The carbon cycle at the ocean margin in the northern Gulf of Biscay. Deep-Sea Res. II, *48*, 3265-3293.

Wong, G.T.F., S.-Y. Chao, Y.-H. Li and F.-K. Shiah. 2000. The Kuroshio edge exchange processes (KEEP) study -an introduction to hypotheses and highlights. Cont. Shelf Res., *20*, 335-347.

Wright, L.D. 1995. Morphodynamics of Inner Continental Shelves, CRC Press, 241 pp.

Xu, J.P., M.A. Noble and L.K. Rosenfeld. 2004. In-situ measurements of velocity structure within turbidity currents. Geophys. Res. Lett., *31(9)*, L09311.

Xu, J.P., M. Noble, S.L. Eittreim, L.K. Rosenfeld, F.B. Schwing and C.H. Pilskaln. 2002. Distribution and transport of suspended particulate matter in Monterey Canyon, California. Mar. Geo., *181*, 215-234.

Figure and Table Captions

Figure 1. Bathymetric map of the northwestern Mediterranean margin. The area is incised by several submarine canyons, some of which, like the Palamós Canyon and the Blanes Canyon, cut the continental shelf at shallow depths. The main regional circulation is also illustrated.

Figure 2. Bathymetric map of the Palamós Canyon and locations of mooring lines used in this study. Each line sustained an Aanderaa RCM-9 current meter equipped with a turbidity sensor at 12 mab. Wave data was provided by an oceanographic buoy and a WANA point (model), also indicated on the map.

Figure 3. Temporal evolution during the study period of a) the Ter River daily discharge at Girona, combined with time series of b) wave peak period (T_P) and c) significant wave height (H_S), recorded by an oceanographic buoy near the Palamós Canyon. Gaps in the buoy time series are filled with values predicted at a nearby WANA point (shaded line).

Figure 4. Net water flows calculated from the north-south and east-west components of the current, measured at 12 mab. a: relatively calm conditions from mid-March through early-November; b: a major storm in November and its aftermath. Current meters M3 (canyon axis, 1200 m depth) and M5 (canyon axis, 1700 m depth) ceased to function at the beginning and end of August respectively.

Figure 5. Progressive vectors calculated from the near-bottom current meters. Crosses indicate the starting point. The initial and final dates are also indicated. Arrows indicate the beginning of the November 11th storm.

Figure 6. Suspended sediment fluxes (SSF) and cumulative mass fluxes in the across- and along-canyon directions at site M2. Positive values are up-canyon and east; negative values are down-canyon and west.

Figure 7. Suspended sediment fluxes (SSF) and cumulative mass fluxes in the across- and along-canyon directions at site M3. Positive values are up-canyon and NNE; negative values are down-canyon and SSW. The time series ended prematurely due to a technical malfunction.

Figure 8. Suspended sediment fluxes (SSF) and cumulative mass fluxes in the across- and along-canyon directions at M5. Positive values are up-canyon and NNE; negative values are down-canyon and SSW. The time series ended prematurely due to a technical malfunction.

Figure 9. Suspended sediment fluxes (SSF) and cumulative mass fluxes in the across- and along-canyon directions at M4. Positive values are up-canyon and NNE; negative values are down-canyon and SSW.

Figure 10. Suspended sediment fluxes (SSF) and cumulative mass fluxes in the across- and along-canyon directions at site M6. Positive values are up-canyon and NE; negative values are down-canyon and SW.

Figure 11. Suspended sediment fluxes (SSF) and cumulative mass fluxes in the across- and along-margin directions at site M7. Data from the first deployment (March-June) are not available.

Figure 12. Current speed, current direction and SSC from selected episodes of increased particle flux at M3 (canyon axis, 1200 m depth). Top graphs (a) show some of the sediment gravity flows triggered by fishing activities and coming from the north canyon wall (modified from Palanques *et al.*, 2006). Bottom graphs (b) illustrate the only 3 major flux peaks flowing downslope along the canyon axis. All graphs are in the same scale. Rose diagrams illustrate the direction of the current during the intervals of increased flux.

Figure 13. Illustration of sediment gravity flows at M5 (a) and M6 (b). Right graphs show suspended sediment concentration measured by the turbidimeter deployed at 12 mab and settling fluxes (TMF) from a sediment trap installed at 22 mab during the study period (Martín *et al.*, 2006). Left graphs are zooms on the most marked nephelometric peaks in each case, showing current direction, current speed, and concentration of suspended particulate matter at 12 mab. Rose diagrams illustrate the direction of the current during the episodes of increased flux.

Figure 14. Net horizontal particle fluxes in the Palamós Canyons and on the adjacent slope at 12 mab, calculated from the available current meter/turbidimeter pairs. a: mid-March through early November; b: November storm period and its aftermath. Current meters M3 and M5 (canyon axis at 1200 and 1700 m depth respectively) ceased to function at the beginning and end of August respectively.

Table 1. Geographical locations, depths and dates of mooring deployments.

Table 2. Maximum and mean velocity modules (cm s^{-1}) recorded by near-bottom (12 mab) current meters. The study is divided into two parts: a period from March through early

November characterized by conditions of low river discharge and relatively low wave heights, and a period comprising the November 11th storm and its aftermath. Not all the mean values cover the same time span, due to premature interruptions of some current meters (see the text and Table 1 for further details).

Figure_1

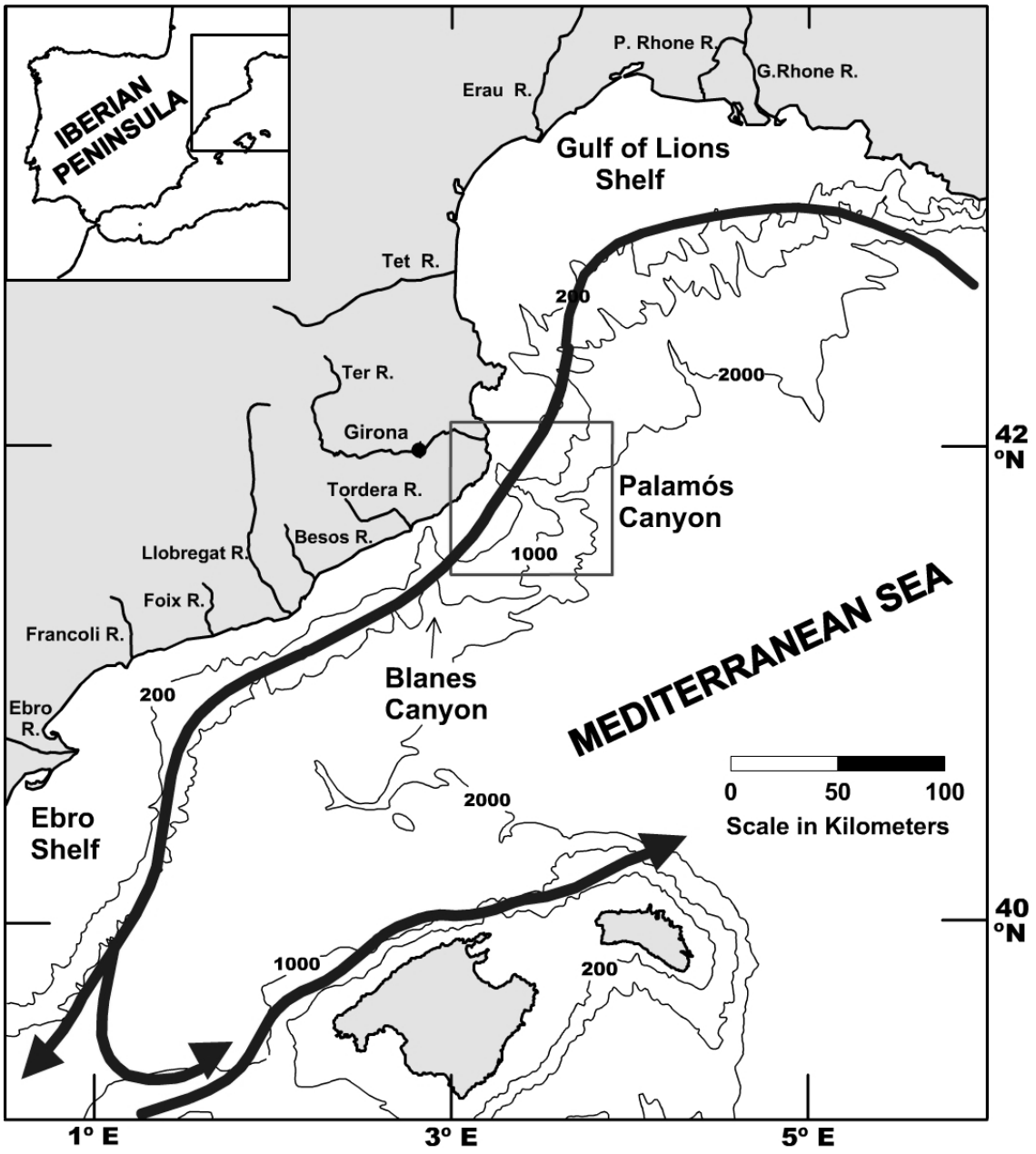
IBERIAN PENINSULA
P. Rhone R.
G.Rhone R.
Erau R.
Gulf of Lions Shelf
Tet R.
200
2000
Ter R.
Girona
Tordera R.
Besos R.
Llobregat R.
Foix R.
Francoli R.
Palamós Canyon
1000
MEDITERRANEAN SEA
Blanes Canyon
200
Ebro R.
Ebro Shelf
2000
0 50 100
Scale in Kilometers
42 ºN
40 ºN
1000
200
1º E
3º E
5º E

Figure_2

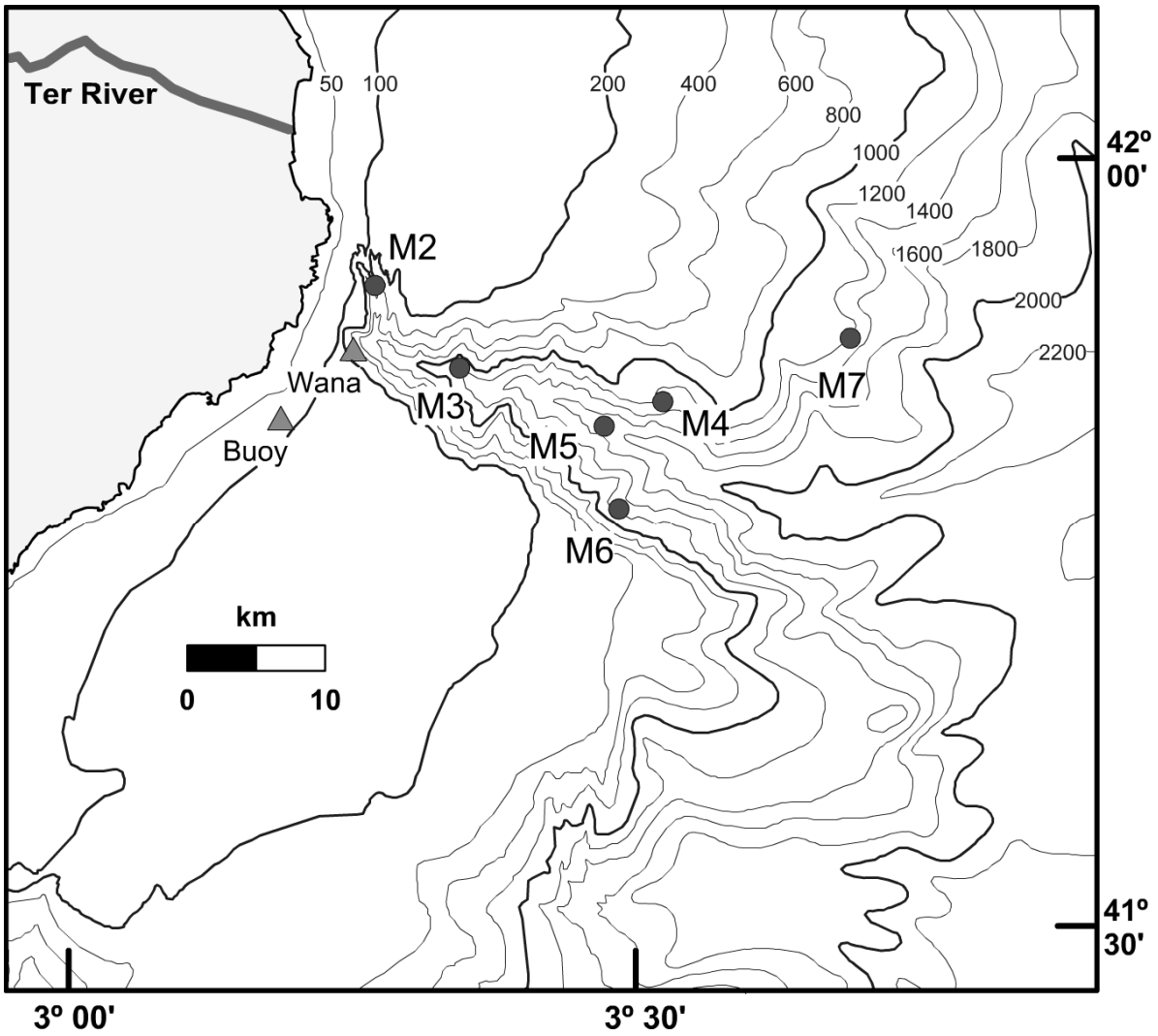
Ter River
50
100
200
400
600
800
1000
1200
1400
1600
1800
2000
2200
M2
M3
M4
M5
M6
M7
Wana
Buoy
km
0
10
42º
00'
41º
30'
3º 00'
3º 30'

Figure_3

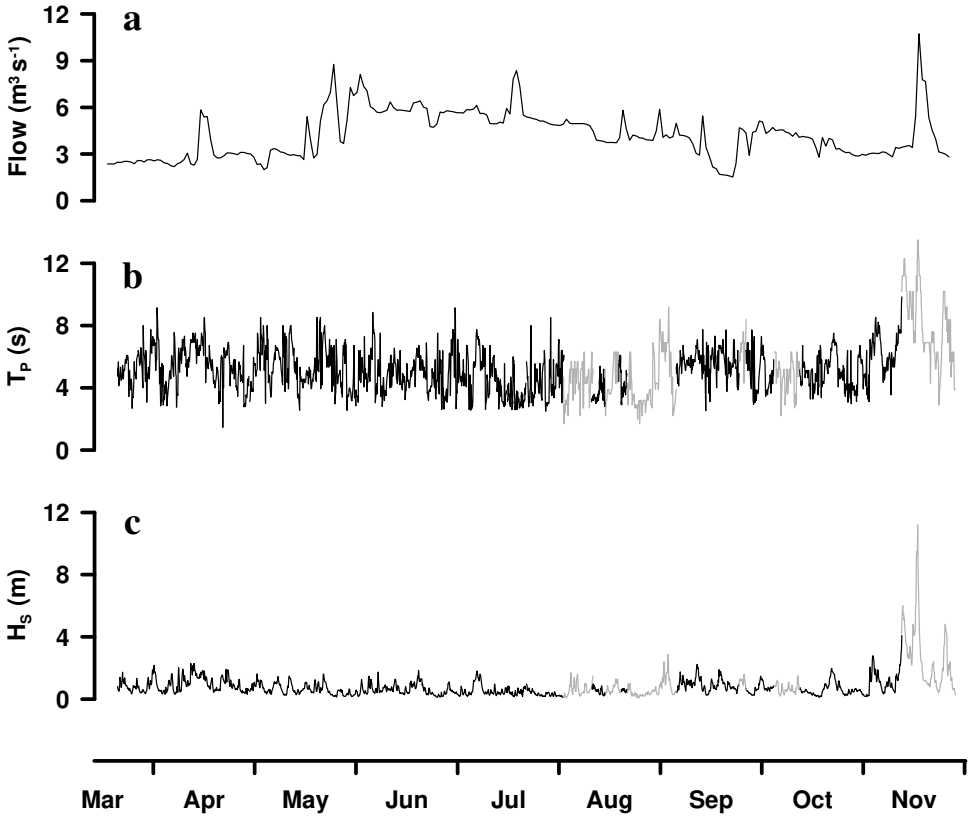
a
b
c
Flow (m³ s⁻¹)
T_P (s)
H_S (m)
12
9
6
3
0
8
4
Mar
Apr
May
Jun
Jul
Aug
Sep
Oct
Nov

Figure_4

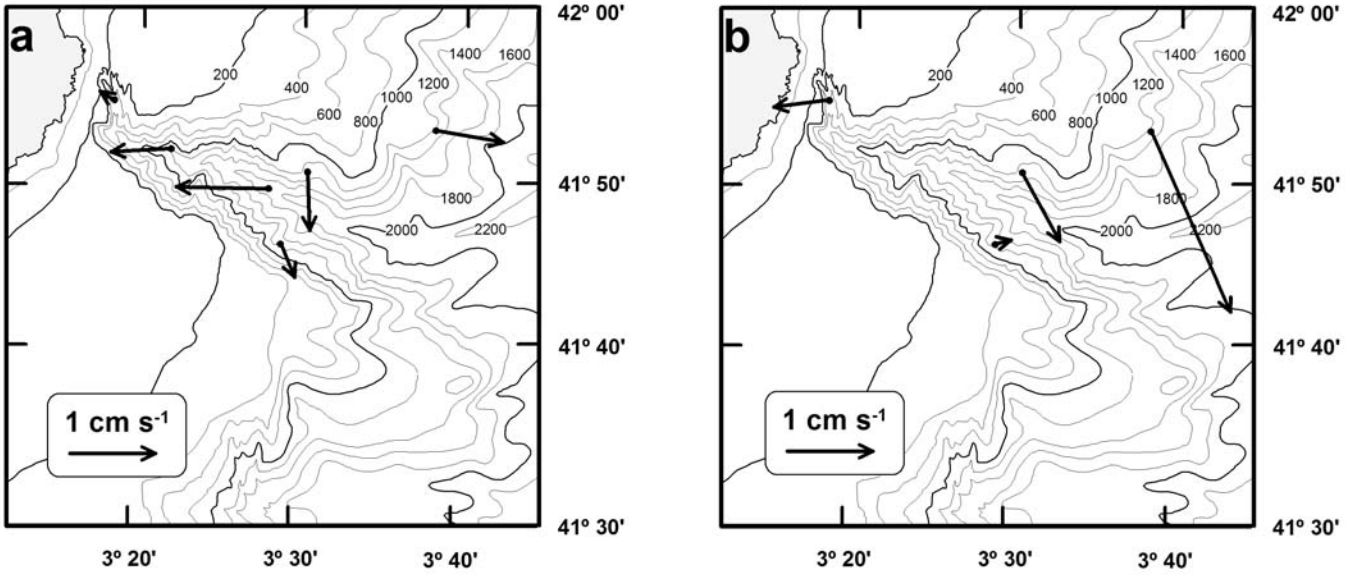
a
b
200
400
600
800
1000
1200
1400
1600
1800
2000
2200
1 cm s-1
42º 00'
41º 50'
41º 40'
41º 30'
3º 20'
3º 30'
3º 40'

Figure_5

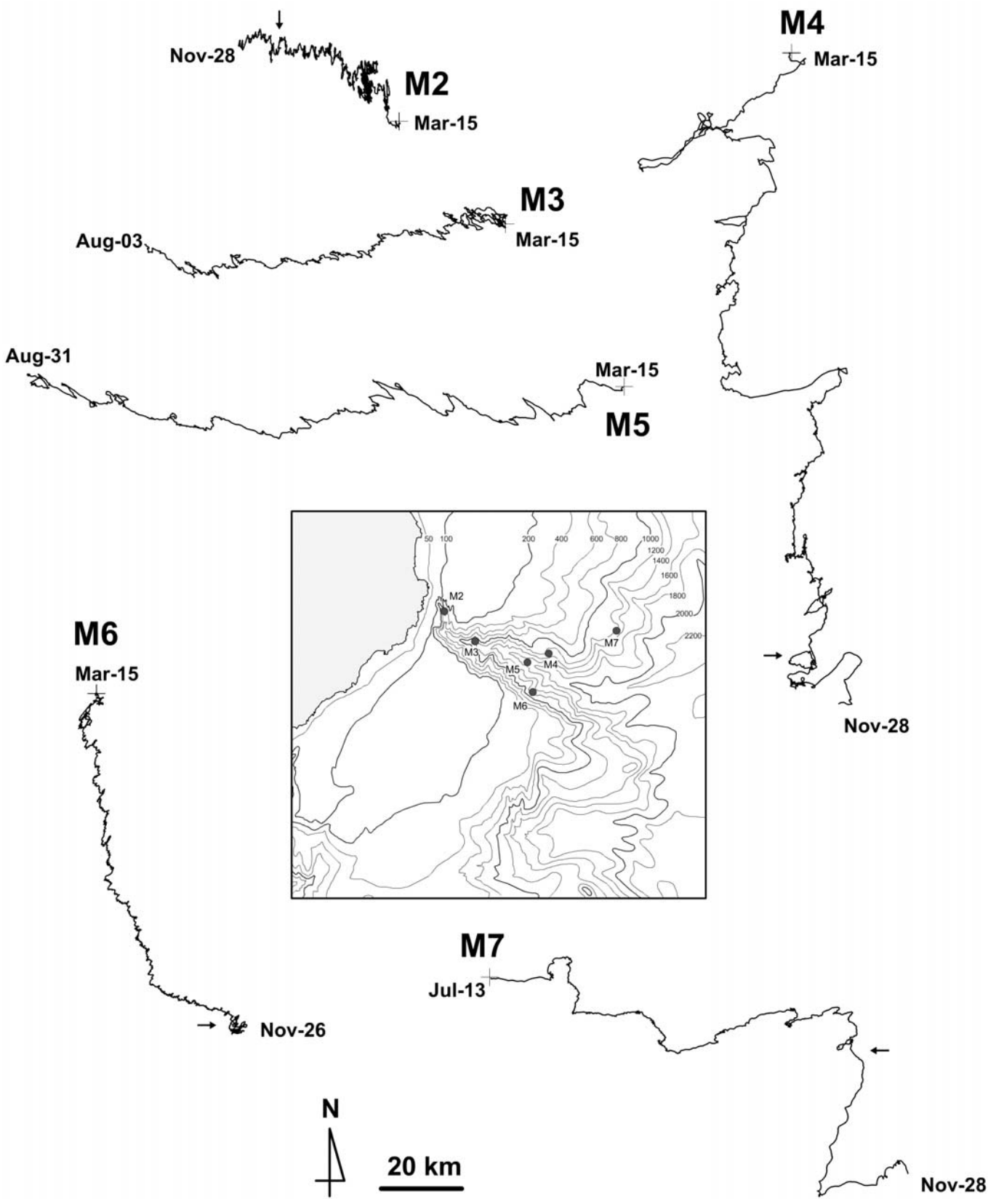
Nov-28
M2
Mar-15
M4
Mar-15
M3
Aug-03
Mar-15
Aug-31
Mar-15
M5
M6
Mar-15
Nov-26
M7
Jul-13
Nov-28
Nov-28
M2
M3
M4
M5
M6
M7
50
100
200
400
600
800
1000
1200
1400
1600
1800
2000
2200
N
20 km

Figure_6

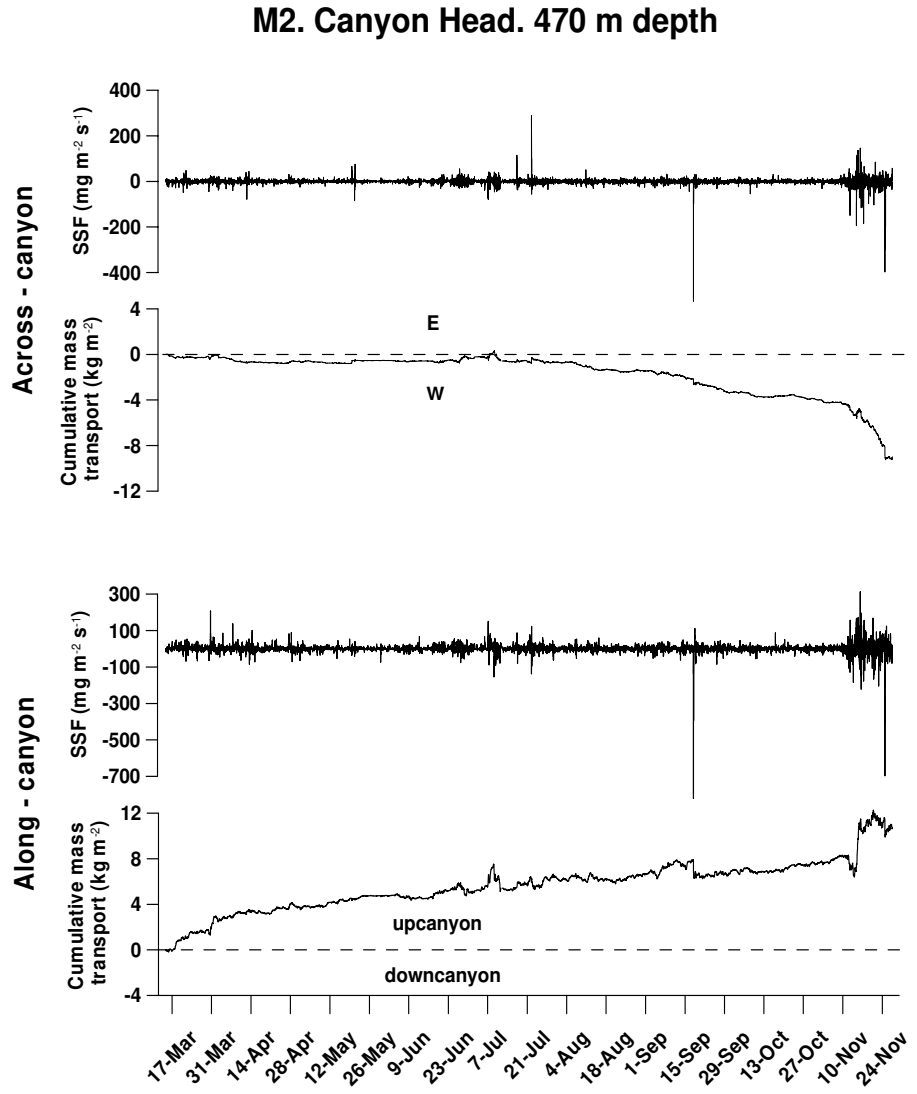
M2. Canyon Head. 470 m depth
Across - canyon
SSF (mg m-2 s-1)
400
200
0
-200
-400
Cumulative mass transport (kg m-2)
4
0
-4
-8
-12
E
W
Along - canyon
SSF (mg m-2 s-1)
300
100
-100
-300
-500
-700
Cumulative mass transport (kg m-2)
12
8
4
0
-4
upcanyon
downcanyon
17-Mar
31-Mar
14-Apr
28-Apr
12-May
26-May
9-Jun
23-Jun
7-Jul
21-Jul
4-Aug
18-Aug
1-Sep
15-Sep
29-Sep
13-Oct
27-Oct
10-Nov
24-Nov

Figure_7

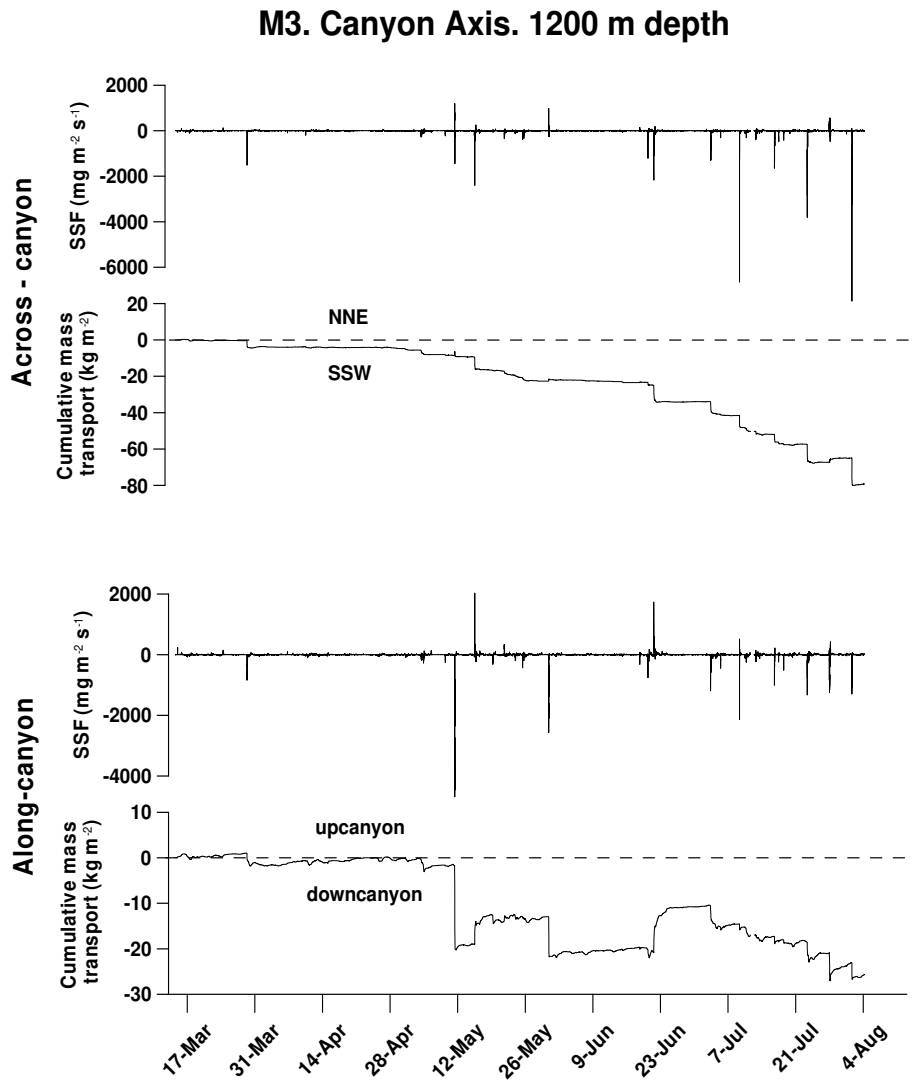
M3. Canyon Axis. 1200 m depth
Across - canyon
SSF (mg m-2 s-1)
2000
0
-2000
-4000
-6000
Cumulative mass transport (kg m-2)
20
0
-20
-40
-60
-80
NNE
SSW
Along-canyon
SSF (mg m-2 s-1)
2000
0
-2000
-4000
Cumulative mass transport (kg m-2)
10
0
-10
-20
-30
upcanyon
downcanyon
17-Mar
31-Mar
14-Apr
28-Apr
12-May
26-May
9-Jun
23-Jun
7-Jul
21-Jul
4-Aug

Figure_8

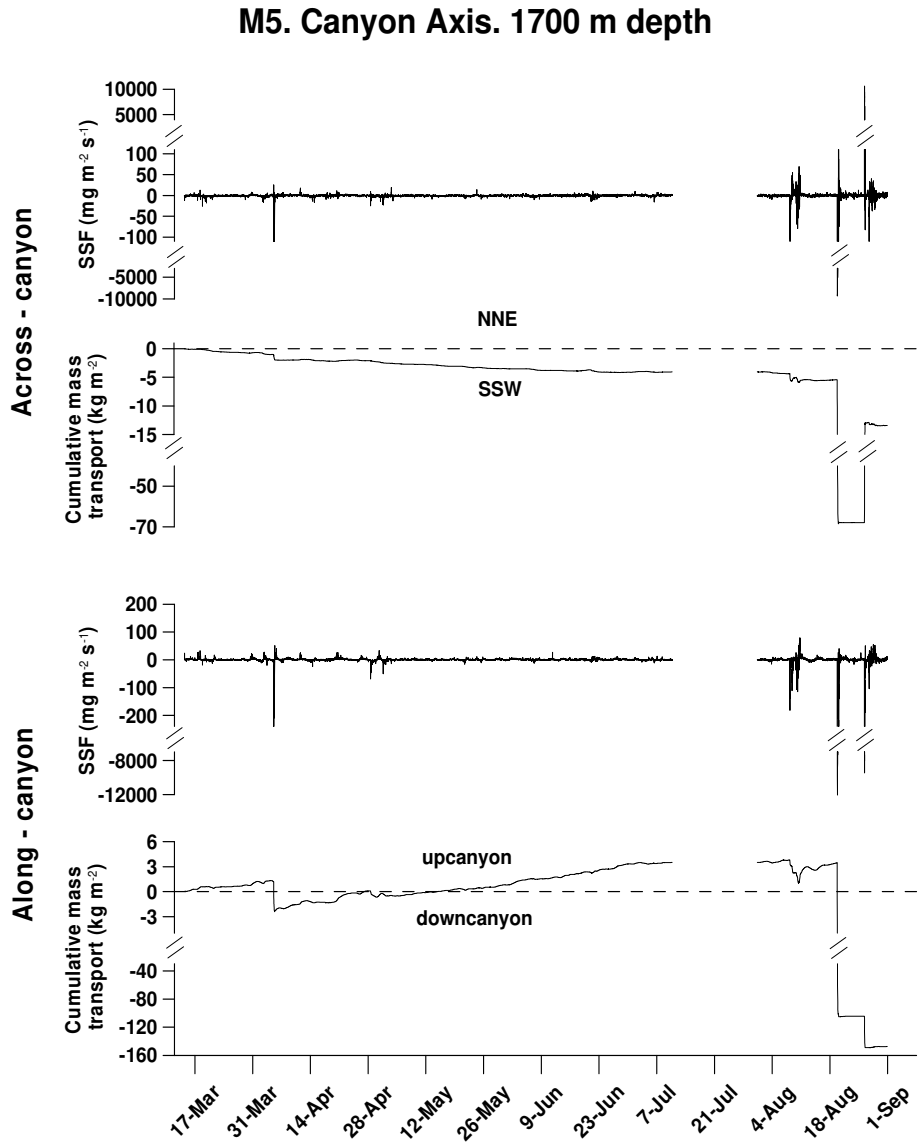
M5. Canyon Axis. 1700 m depth
Across - canyon
SSF (mg m-2 s-1)
10000
5000
100
50
0
-50
-100
-5000
-10000
NNE
SSW
Cumulative mass transport (kg m-2)
0
-5
-10
-15
-50
-70
Along - canyon
SSF (mg m-2 s-1)
200
100
0
-100
-200
-8000
-12000
upcanyon
downcanyon
Cumulative mass transport (kg m-2)
6
3
0
-3
-40
-80
-120
-160
17-Mar
31-Mar
14-Apr
28-Apr
12-May
26-May
9-Jun
23-Jun
7-Jul
21-Jul
4-Aug
18-Aug
1-Sep

Figure_9

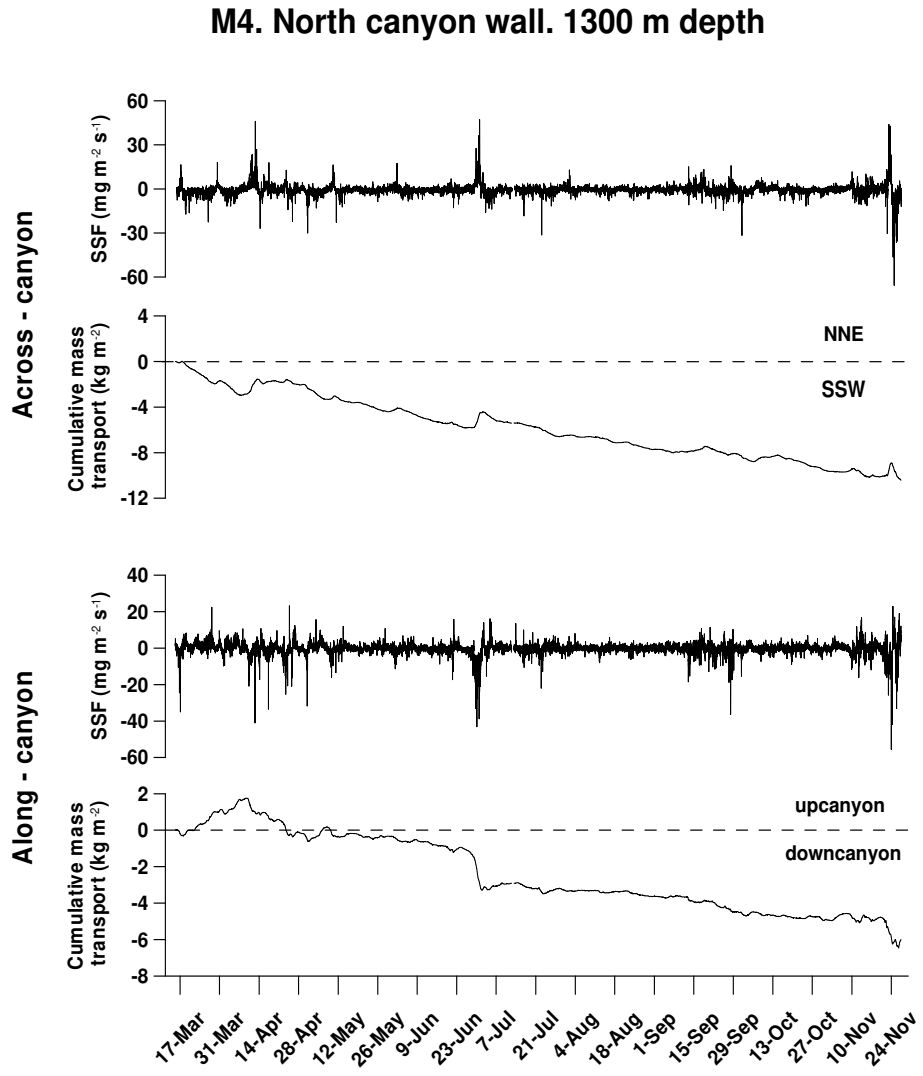
M4. North canyon wall. 1300 m depth
Across - canyon
SSF (mg m-2 s-1)
60
30
0
-30
-60
Cumulative mass transport (kg m-2)
4
0
-4
-8
-12
NNE
SSW
Along - canyon
SSF (mg m-2 s-1)
40
20
0
-20
-40
-60
Cumulative mass transport (kg m-2)
2
0
-2
-4
-6
-8
upcanyon
downcanyon
17-Mar
31-Mar
14-Apr
28-Apr
12-May
26-May
9-Jun
23-Jun
7-Jul
21-Jul
4-Aug
18-Aug
1-Sep
15-Sep
29-Sep
13-Oct
27-Oct
10-Nov
24-Nov

Figure_10

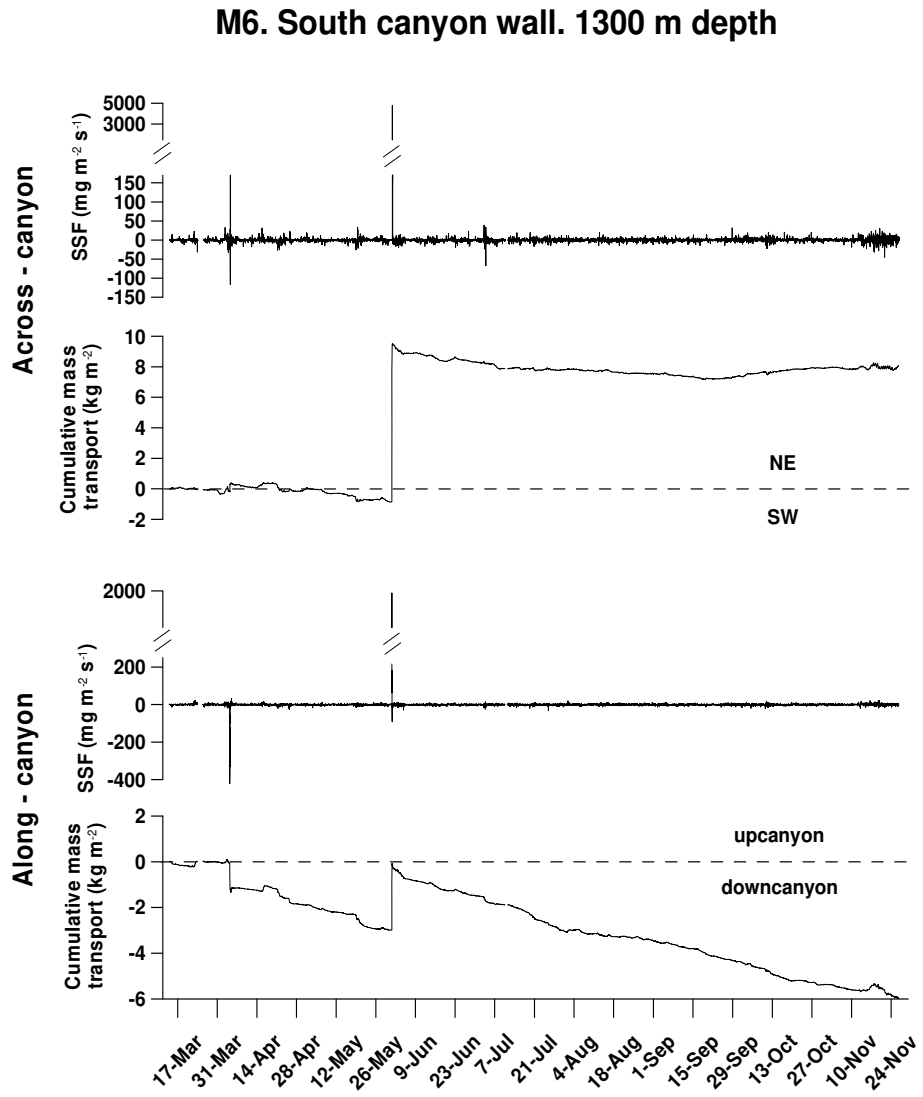
M6. South canyon wall. 1300 m depth
Across - canyon
SSF (mg m-2 s-1)
5000
3000
150
100
50
0
-50
-100
-150
Cumulative mass transport (kg m-2)
10
8
6
4
2
0
-2
NE
SW
Along - canyon
SSF (mg m-2 s-1)
2000
200
0
-200
-400
Cumulative mass transport (kg m-2)
2
0
-2
-4
-6
upcanyon
downcanyon
17-Mar
31-Mar
14-Apr
28-Apr
12-May
26-May
9-Jun
23-Jun
7-Jul
21-Jul
4-Aug
18-Aug
1-Sep
15-Sep
29-Sep
13-Oct
27-Oct
10-Nov
24-Nov

Figure_11

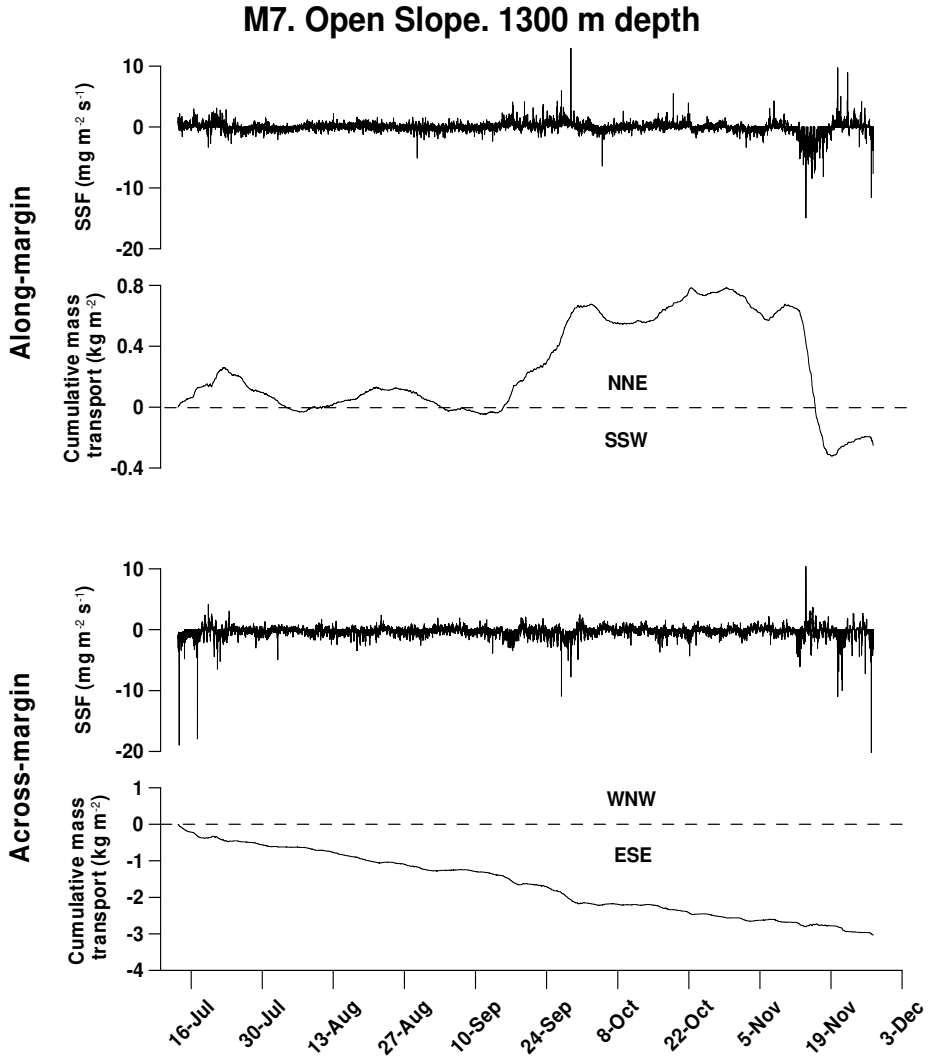
M7. Open Slope. 1300 m depth
Along-margin
SSF (mg m-2 s-1)
10
0
-10
-20
Cumulative mass transport (kg m-2)
0.8
0.4
0
-0.4
NNE
SSW
Across-margin
SSF (mg m-2 s-1)
10
0
-10
-20
Cumulative mass transport (kg m-2)
1
0
-1
-2
-3
-4
WNW
ESE
16-Jul
30-Jul
13-Aug
27-Aug
10-Sep
24-Sep
8-Oct
22-Oct
5-Nov
19-Nov
3-Dec

Figure_12

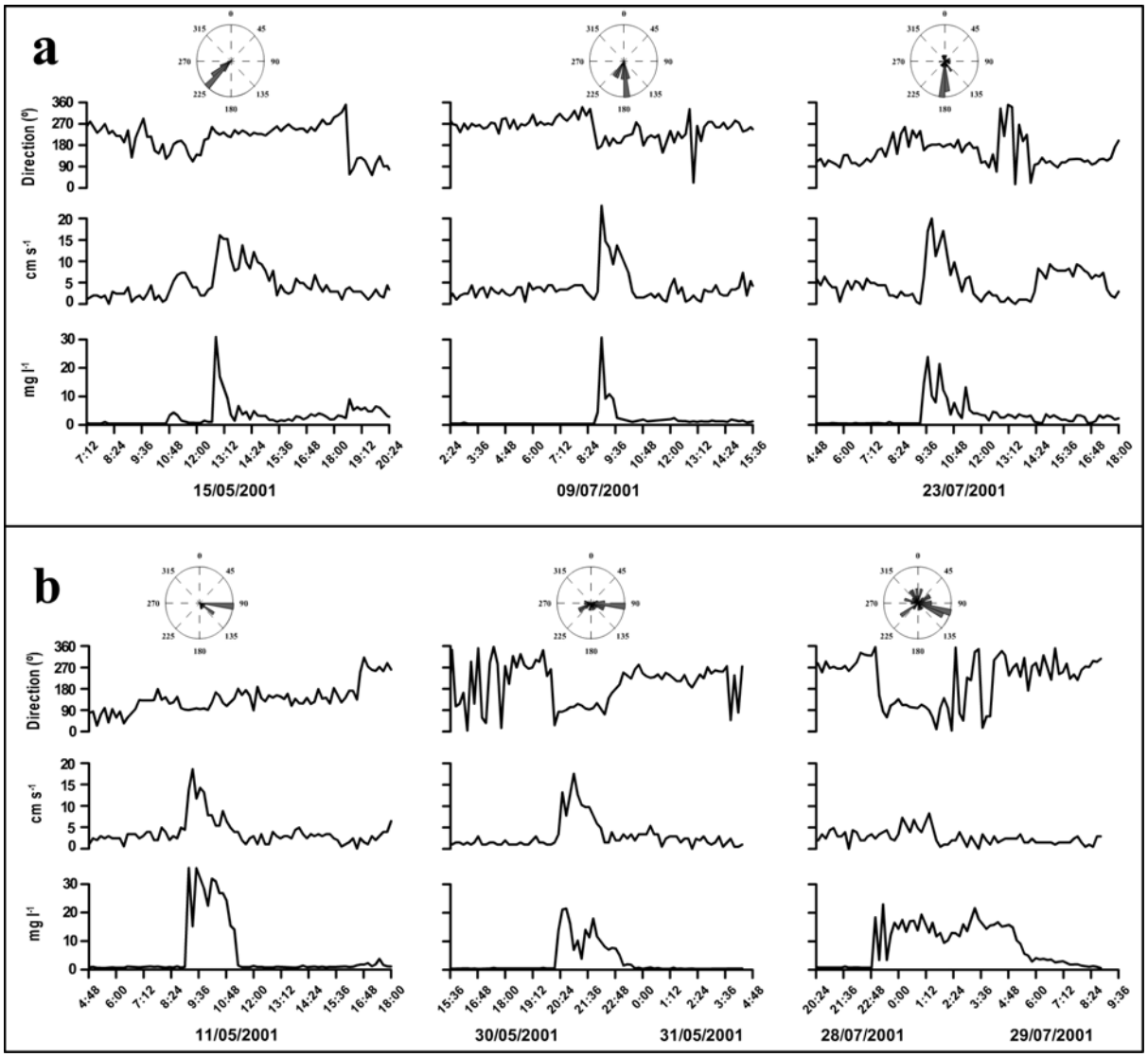
a
Direction (°)
cm s-1
mg l-1
15/05/2001
09/07/2001
23/07/2001
b
Direction (°)
cm s-1
mg l-1
11/05/2001
30/05/2001
31/05/2001
28/07/2001
29/07/2001

Figure_13

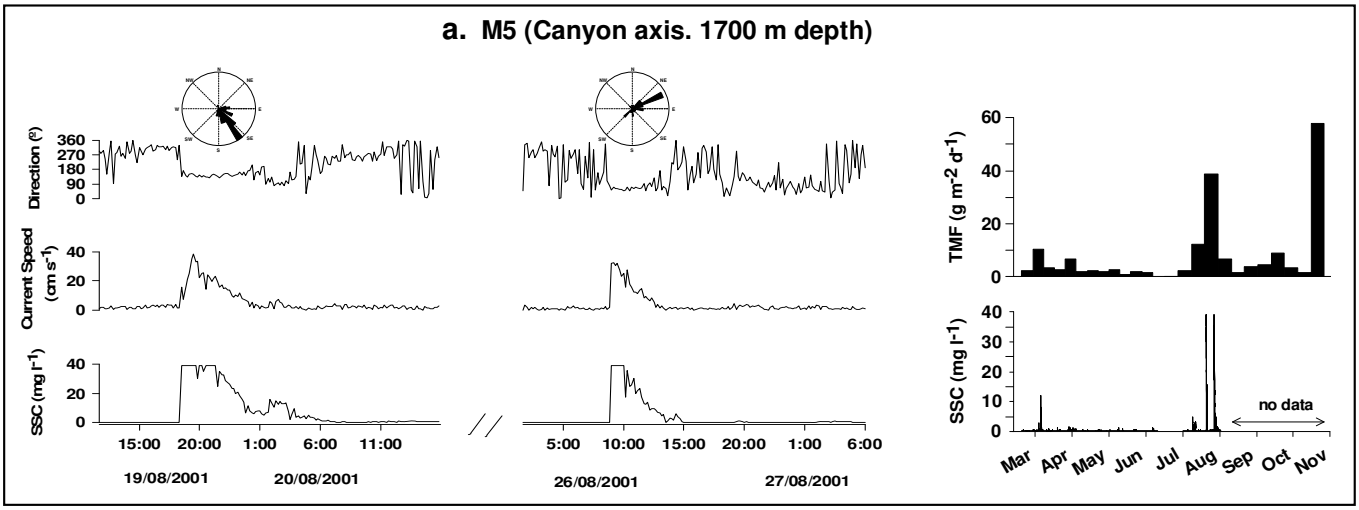
a. M5 (Canyon axis. 1700 m depth)
Direction (º)
360
270
180
90
0
Current Speed (cm s-1)
40
20
0
SSC (mg l-1)
40
20
0
15:00
20:00
1:00
6:00
11:00
19/08/2001
20/08/2001
5:00
10:00
15:00
20:00
1:00
6:00
26/08/2001
27/08/2001
TMF (g m-2 d-1)
60
40
20
0
SSC (mg l-1)
40
30
20
10
0
no data
Mar
Apr
May
Jun
Jul
Aug
Sep
Oct
Nov

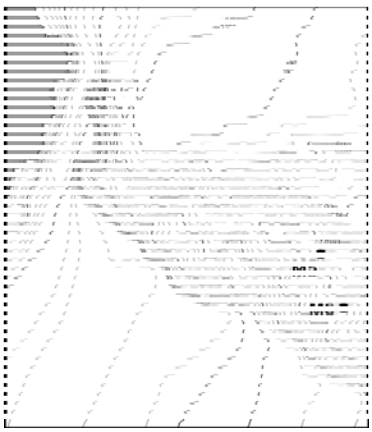

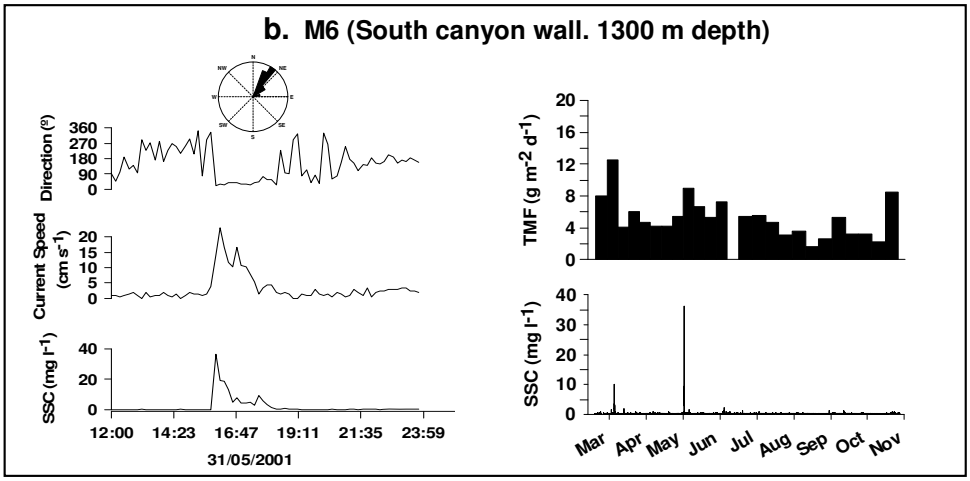
b. M6 (South canyon wall. 1300 m depth)
Direction (º)
360
270
180
90
0
Current Speed (cm s-1)
20
15
10
5
0
SSC (mg l-1)
40
20
0
12:00
14:23
16:47
19:11
21:35
23:59
31/05/2001
TMF (g m-2 d-1)
20
16
12
8
4
0
SSC (mg l-1)
40
30
20
10
0
Mar
Apr
May
Jun
Jul
Aug
Sep
Oct
Nov

Figure_14

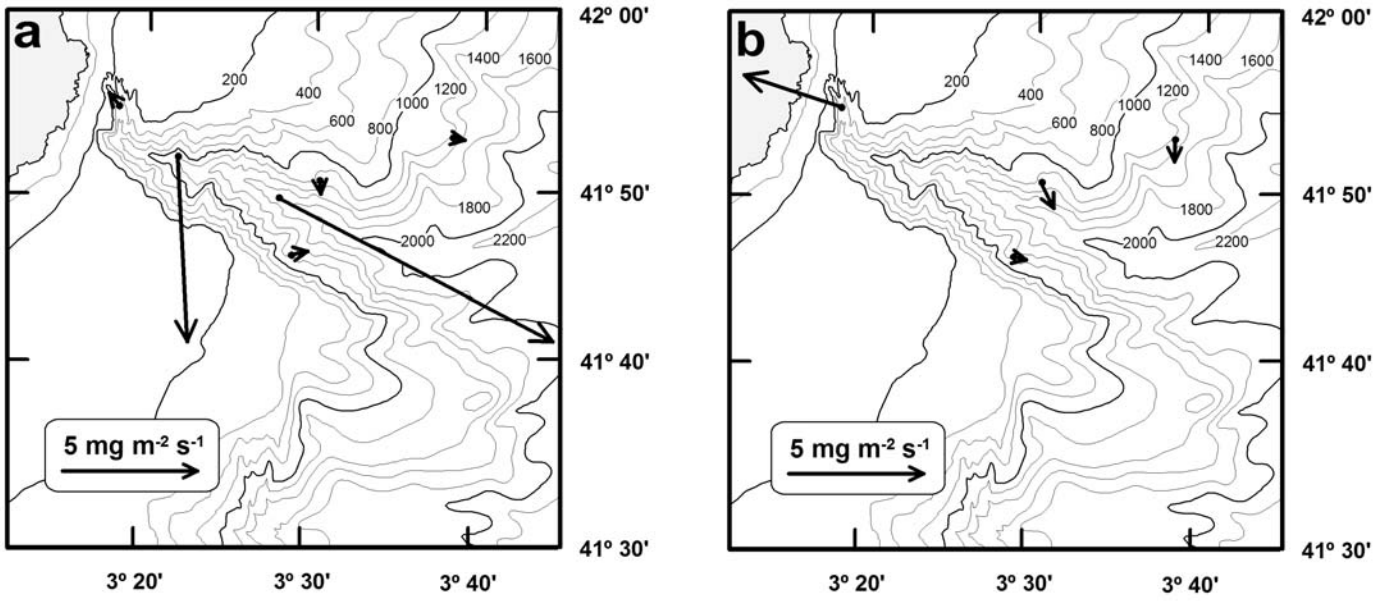
a
b
200
400
600
800
1000
1200
1400
1600
1800
2000
2200
5 mg m-2 s-1
42º 00'
41º 50'
41º 40'
41º 30'
3º 20'
3º 30'
3º 40'

Table_1

Mooring	Deployment	Longitude	Latitude	Depth (m)	Dates
M2	1st	3º16'19.0''E	41º55'19.8''N	470	14/03-11/07/2001
	2nd	3º16'06.6''E	41º55'28.8''N	470	12/07-28/11/2001
M3	1st	3º20'47.4''E	41º52'01.2''N	1166	14/03-11/07/2001
	2nd	3º20'46.2''E	41º52'02.4''N	1206	12/07-04/08/2001
M4	1st	3º31'01.5''E	41º50'22.9''N	1301	15/03-12/07/2001
	2nd	3º31'12.6''E	41º50'43.8''N	1299	13/07-28/11/2001
M5	1st	3º27'49.2''E	41º50'03.0''N	1728	14/03-10/07/2001
	2nd	3º27'52.2''E	41º49'39.5''N	1747	31/07-31/08/2001
M6	1st	3º28'46.2''E	41º46'20.3''N	1338	13/03-10/07/2001
	2nd	3º28'40.2''E	41º46'36.6''N	1292	11/07-26/11/2001
M7	1st	3º41'19.2''E	41º53'16.8''N	1322	15/03-12/07/2001
	2nd	3º40'57.6''E	41º53'22.8''N	1271	13/07-28/11/2001

Table_2

	Calm conditions Mar 13 / Nov 10 - 2001		Stormy period Nov 11 / Nov 28 - 2001	
Mooring	Mean	Max.	Mean	Max.
M2	3.1	29.3	5.6	37.6
M3	3.0	24.4	-	-
M4	2.8	18.6	5.5	16.6
M5	2.6	38.1	-	-
M6	1.9	23.0	3.7	13.2
M7	2.1	9.3	5.4	17.1